

An improved particle swarm optimization algorithm and its application to search for new magnetic ground states in the Hubbard model

Ze Ruan,^{1,*} Xiu-Cai Jiang,^{1,*} Ze-Yi Song,¹ and Yu-Zhong Zhang^{1,†}

¹*Shanghai Key Laboratory of Special Artificial Microstructure Materials and Technology, School of Physics Science and engineering, Tongji University, Shanghai 200092, P.R. China*

(Dated: March 14, 2024)

An improved particle swarm optimization algorithm is proposed and its superiority over standard particle swarm optimization algorithm is tested on two typical benchmark functions. By employing this algorithm to search for the magnetic ground states of the Hubbard model on the real-space square lattice with finite size based on the mean-field approximation, two new magnetic states, namely the double striped-type antiferromagnetic state and the triple antiferromagnetic state, are found. We further perform mean-field calculations in the thermodynamical limit to confirm that these two new magnetic states are not a result of a finite-size effect, where the properties of the double striped-type antiferromagnetic state are also presented.

I. INTRODUCTION

Antiferromagnetism has attracted tremendous interests due to the fact that the parent states of cuprates and iron-based superconductors are either antiferromagnets or paramagnets with antiferromagnetic fluctuations, such as the checkerboard antiferromagnetic (CAF) insulator of cuprates, nearly degenerate double-stripe (DAF) and plaquette antiferromagnetic (PAF) order in FeTe^{1,2}, pair-checkerboard antiferromagnetic (PCAF) order in monolayer FeSe thin film^{3,4}, molecular-intercalated FeSe⁵, and A_xFe_{2-y}Se₂⁶, as well as stripe-type antiferromagnetic (SAF) order in other iron-based mother materials⁷⁻⁹, which indicates a magnetic origin of the two high- T_c unconventional superconductors.

Therefore, much effort has been spent on studying the properties of these magnetic states based on models related to these two superconducting families. A simple Heisenberg model with the nearest and next-nearest neighbour intralayer couplings has been used to explain the transition from CAF to SAF¹⁰. Additionally, a combination of this simple Heisenberg model with the third-neighbour intralayer coupling solely^{11,12}, or with three couplings¹³, namely the third-neighbour intralayer coupling, nearest interlayer coupling, and intralayer nearest-neighbour biquadratic coupling, is introduced to further include DAF and PAF. In addition to these models, an effective orbital-degenerate double-exchange model consisting of both itinerant electrons and localized spins is used to take CAF, DAF, and SAF into consideration¹⁴. Alternatively, the Hubbard model which covers both weak and strong coupling limits for magnetism is also employed to investigate these magnetic states, for example, the single-orbital Hubbard model with the nearest and next-nearest neighbour hoppings. Using methods like variational cluster approximation^{15,16}, variational Monte Carlo¹⁷, and mean-field theory¹⁸, the presence of CAF and SAF in this model is proposed. Apart from these two states, PCAF is also found in this model by path-integral renormalization group method¹⁹ and variational cluster approximation²⁰. Recently, it has been pointed

out that this Hubbard model can serve as a unified minimal model to describe all the magnetic states mentioned above²¹.

However, despite numerous investigations, only a few new magnetic states which probably exist in the experiment are predicted based on the aforementioned superconductor-related magnetic models. For example, the spiral and staggered trimer states are predicted in J_1 - J_2 - J_3 - K Heisenberg model²², or a spiral state is found in a frustrated Hubbard model containing the nearest and next-nearest neighbour hoppings, where the latter hopping breaks C_4 symmetry²³. The lack of new magnetic states may be due to the weakness of conventional methods, such as variational cluster approximation, variational Monte Carlo, mean-field theory, etc., as they require preparation of the desired configurations while it is impossible to exhaust all magnetic patterns. Thus, a natural question arises: whether more new exotic magnetic states occur in the aforementioned unified minimal Hubbard model using a method superior to conventional methods? Noticeably, the particle swarm optimization (PSO) algorithm is proven to be a powerful approach^{24,25}, which is also used in the prediction of new materials²⁶⁻²⁹ and the estimation of cosmological parameters^{30,31}, etc. Regarding that PSO can handle problems with numerous energy minima²⁶ and generate random particles, it may be suitable to search for new magnetic states, where a magnetic pattern is viewed as a particle. Nevertheless, the insufficient performance of standard PSO that sometimes converges slowly³² or tends to converge to local minima³³ impedes such application. Although lots of attempts have been undertaken to improve the performance of the standard PSO³⁴⁻⁴¹, an improved PSO with the hyperparameters (including the inertia weight and learning factors) depending on individual character of particle has not yet been proposed. Therefore, proposing an improved PSO with particle-dependent hyperparameters and using it to search for new magnetic states in the aforementioned Hubbard model is an interesting work.

In this paper, we proposed an improved PSO, where

the hyperparameters of a specific particle depend on its present position, corresponding local best, and global best. We first show the superiority of this improved PSO over standard PSO on two typical benchmark functions, namely the Griewank function and Rastrigrin function. Then, by employing this improved PSO to search for the magnetic ground state of the Hubbard model on the real-space square lattice with a finite size of 24×24 based on the mean-field approximation, two new magnetic states are found, namely the double stripe-type state (DSAF) and the triple antiferromagnetic state (TAF). By comparing the free energies of these two new states with their competing states in corresponding parameter space using mean-field theory in the thermodynamical limit, we further confirm that these two new magnetic states are not a result of a finite-size effect. Besides, we present the properties of DSAF which occurs at a region of weak frustration.

Our paper is organized as follows. Section II describes the Hubbard model and the standard PSO. Section III presents our main results, including the superiority of our improved PSO over the standard PSO, the search of new magnetic ground states of Hubbard model on the square lattice with a finite real-space size using improved PSO, and the mean-field calculations in the thermodynamical limit. Section IV presents a detailed discussion, and Section V concludes with a summary.

II. MODEL AND METHOD

The Hubbard model on a square lattice with the nearest and next-nearest neighbour hoppings we studied is given by

$$H = -t_1 \sum_{\langle i,j \rangle, \sigma} c_{i\sigma}^\dagger c_{j\sigma} - t_2 \sum_{\langle\langle i,j \rangle\rangle, \sigma} c_{i\sigma}^\dagger c_{j\sigma} + U \sum_i n_{i\uparrow} n_{i\downarrow}, \quad (1)$$

where $c_{i\sigma}^\dagger$ ($c_{i\sigma}$) creates (annihilates) an electron at site i with spin σ . $n_{i\sigma}$ is the number operator. t_1 and t_2 denote the nearest- and next-nearest-neighbour hoppings, and U is the on-site Coulomb interaction. $\langle i, j \rangle$ ($\langle\langle i, j \rangle\rangle$) means the summation over nearest (next-nearest)-neighbor sites. The on-site Coulomb interaction is treated by mean-field approximation as

$$U n_{i\uparrow} n_{i\downarrow} \approx U n_{i\uparrow} \langle n_{i\downarrow} \rangle + U \langle n_{i\uparrow} \rangle n_{i\downarrow} - U \langle n_{i\uparrow} \rangle \langle n_{i\downarrow} \rangle. \quad (2)$$

By defining respectively the magnetic moment and charge occupation of i site as $m_i = \langle n_{i\uparrow} \rangle - \langle n_{i\downarrow} \rangle$ and $\bar{n}_i = \langle n_{i\uparrow} \rangle + \langle n_{i\downarrow} \rangle$, we have

$$\langle n_{i\uparrow} \rangle = \frac{1}{2}(\bar{n}_i + m_i), \quad \langle n_{i\downarrow} \rangle = \frac{1}{2}(\bar{n}_i - m_i). \quad (3)$$

Thus, for a given charge distribution and magnetic configuration $\{\bar{n}_1, \dots, \bar{n}_N, m_1, \dots, m_N\}$, the free energy can be calculated as

$$F = -\frac{1}{\beta} \ln \Xi + \sum_{i=1}^N \left(\mu + \frac{U m_i^2}{4} - \frac{U \bar{n}_i^2}{4} \right), \quad (4)$$

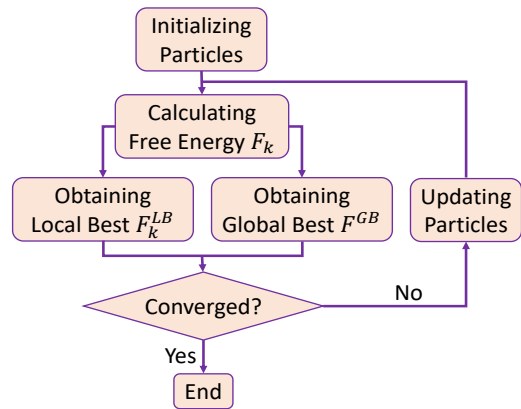


FIG. 1. The flowchart of PSO, where local best and global best are the minimal free energy of k -th particle and all particles, respectively. When the convergence criterion is reached, $|F_k^{LB} - F^{GB}| < \epsilon$ satisfies for any given k -th particle, where ϵ is a small positive number.

in which the grand partition function reads

$$\ln \Xi = \sum_{\sigma} \sum_{i=1}^N \ln \left[1 + e^{-\beta(E_{i\sigma} - \mu)} \right], \quad (5)$$

where N is the total number of sites in the system, β is the inversed temperature defined as $1/(k_B T)$, μ denotes the chemical potential, and $E_{i\sigma}$ is the eigenvalue derived by diagonalizing the Hamiltonian matrix of the system. Specifically, for the case with uniform charge distribution at half-filling, namely $\bar{n}_1 = \dots = \bar{n}_N = 1$, the free energy is a function of the magnetic configuration $\{m_1, \dots, m_N\}$.

We proceed to demonstrate how this Hubbard model is solved within the framework of PSO based on the mean-field approximation, where a magnetic configuration is viewed as a particle and free energy F is the target function to be optimized to a minimum value. The flowchart of PSO is shown in Fig.1. As can be seen, the first iteration consists of following 4 steps while other iterations contain the last 3 of these steps within the framework of PSO:

- (i) Initializing randomly particles, namely a set of magnetic configurations $\{X_1, \dots, X_k, \dots, X_P\}$, where $X_k = \{m_1^k, \dots, m_N^k\}$ and P is the total number of particles.
- (ii) Calculating the free energies of these magnetic configurations $\{F_1, \dots, F_k, \dots, F_P\}$ according to Eq.(4).
- (iii) Evaluating local best $\{F_1^{LB}, \dots, F_k^{LB}, \dots, F_P^{LB}\}$ and global best F^{GB} based on $\{F_1, \dots, F_k, \dots, F_P\}$ of current and last iterations.
- (iv) Determining whether the convergence criterion is reached. If $|F_k^{LB} - F^{GB}| < \epsilon$ satisfies for any given k -th particle, where ϵ is a small positive number, the calculation is completed, otherwise, updating the magnetic configurations and turning to step (ii) using the following equations

$$\begin{cases} D_k^{New} = \omega D_k^{Old} + c_1 r_1 (X_k^{LB} - X_k) + c_2 r_2 (X^{GB} - X_k) \\ X_k^{New} = X_k + D_k^{New} \end{cases}, \quad (6)$$

where ω denotes the inertia weight, c_1 and c_2 are the learning factors, and $r_1(r_2)$ is a random number between 0 and 1 that vary at each iteration. X_k^{LB} and X_k^{GB} are the magnetic configurations of local best and global best, respectively. D_k^{New} and D_k^{Old} denote separately the displacement between the new and current k-th magnetic configurations, and that between the current and last k-th magnetic configurations, in which D_k^{Old} should be initialized at the first iteration. It is necessary to mention that, for standard PSO, c_1 , c_2 , and ω are particle-independent, where c_1 and c_2 are two constants while ω decreases linearly at first and then remains a small value with the proceeding of iteration.

In contrast to standard PSO, the learning factors and inertia weight of our improved PSO are particle-dependent, where c_1 and c_2 have the forms

$$c_{1k} = \frac{e^{F_k^{GB}}}{e^{F_k^{GB}} + e^{F_k^{LB}}}, \quad c_{2k} = \frac{e^{F_k^{LB}}}{e^{F_k^{GB}} + e^{F_k^{LB}}}, \quad (7)$$

while ω reads

$$\omega_k = \begin{cases} \xi & (F_k \leq F_k^{GB} \cap F_k \leq F_k^{LB}) \\ (F_k - F_k^{GB})^\gamma & (F_k^{GB} < F_k < F_k^{LB}) \\ (2F_k - F_k^{GB} - F_k^{LB})^\gamma & (F_k^{GB} < F_k \cap F_k^{LB} < F_k) \end{cases}, \quad (8)$$

in which γ is a tunable positive number with the highest performance when $1.5 \sim 1.7$ for Rastrigrin function, $5 \sim 7$ for the Griewank function, and 0.01 for this Hubbard model while ξ is a small positive number. Thus, by combining equations (4)-(8), the Hubbard model can be solved self-consistently using our improved PSO.

III. RESULTS

A. The superiority of our improved PSO over standard PSO

We will now investigate the superiority of our improved PSO over standard PSO on two typical benchmark functions, namely the Griewank function and Rastrigrin function. As we have proposed the improved version for both the learning factors and inertia weight in our improved PSO, it is necessary to use the controlled variable method to separately investigate the performance improvement for standard PSO when including the learning factors or inertia weight individually.

In Fig.2, we compare the convergence process on the Griewank function [2(a)] and Rastrigrin function [2(b)] using PSO with improved c_1 and c_2 or with standard c_1 and c_2 , where the inertia weight of standard PSO is used. Obviously, for these two typical benchmark functions, the convergence process of PSO using our improved version of c_1 and c_2 converges faster than that using c_1 and c_2 of standard PSO in a wide range of parameter space, indicating the superiority of our improved PSO over standard PSO regarding the learning factors.

Furthermore, we compare the convergence process on the Griewank function and Rastrigrin function in

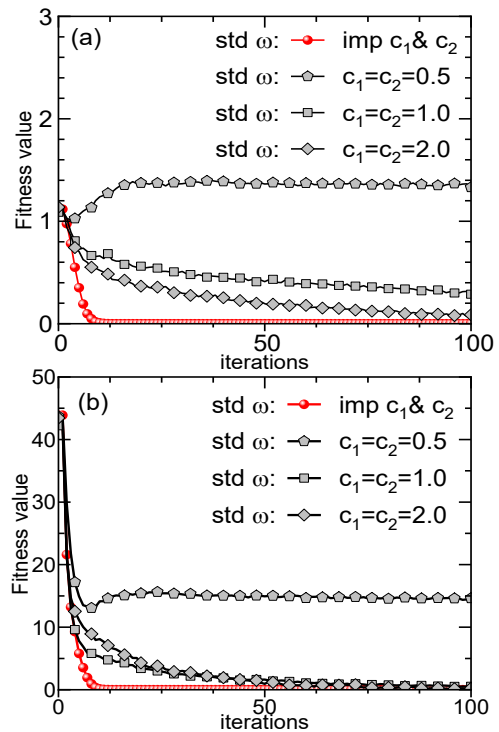


FIG. 2. The convergence process on the Griewank function (a) and Rastrigrin function (b) using PSO with improved c_1 and c_2 or with standard c_1 and c_2 where the inertia weight (ω) of standard PSO is used.

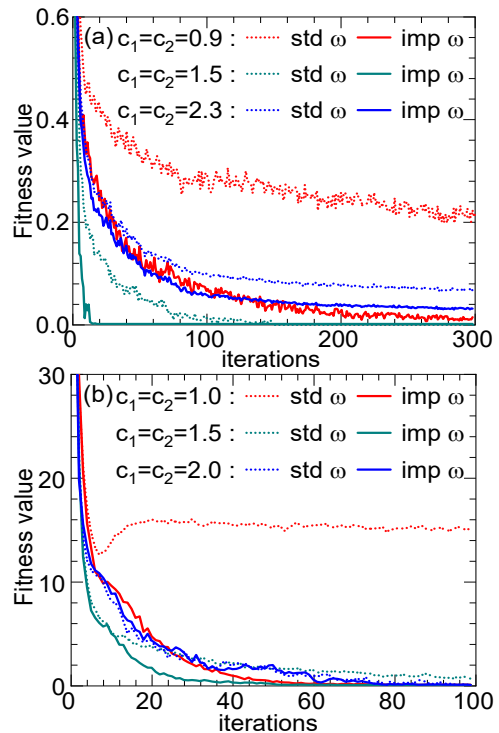


FIG. 3. The convergence process on the Griewank function (a) and Rastrigrin function (b) using PSO with improved ω or with standard ω where the learning factors (c_1 and c_2) of standard PSO are used.

Fig.3(a) and 3(b), respectively, using PSO with the improved version of ω or with the standard version of ω , where the learning factors of standard PSO are used. Similarly, our improved version of ω exhibits higher performance than the standard version of ω in wide range of c_1 and c_2 for these two typical benchmark functions.

Thus, for both learning factors and inertia weight, our improved versions exhibit a higher performance than the standard PSO. It is necessary to mention that the combination of these two kinds of improved hyperparameters converges faster than the inclusion of learning factors or inertia weight individually.

B. The application of improved PSO in the Hubbard model

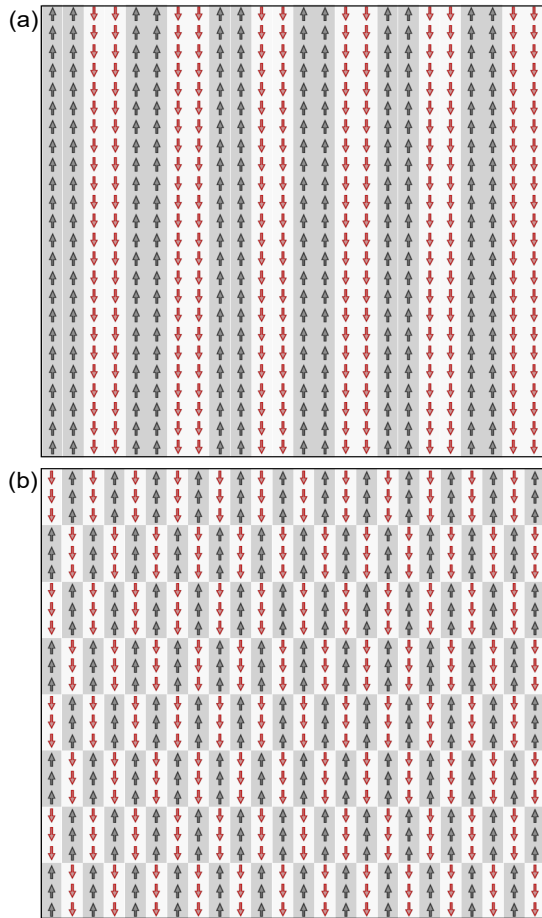


FIG. 4. The DASF and TAF patterns found by our improved PSO on the real-space square lattice with a finite size of 24×24 , where $t_2/t_1 = 0.99$ and $U/t_1 = 3.4$ in (a) while $t_2/t_1 = 0.765$ and $U/t_1 = 4.43$ in (b).

We then employ our improved PSO to search for new magnetic ground states of the Hubbard model on the real-space square lattice with a finite size of 24×24 based on the mean-field approximation. Periodical boundary

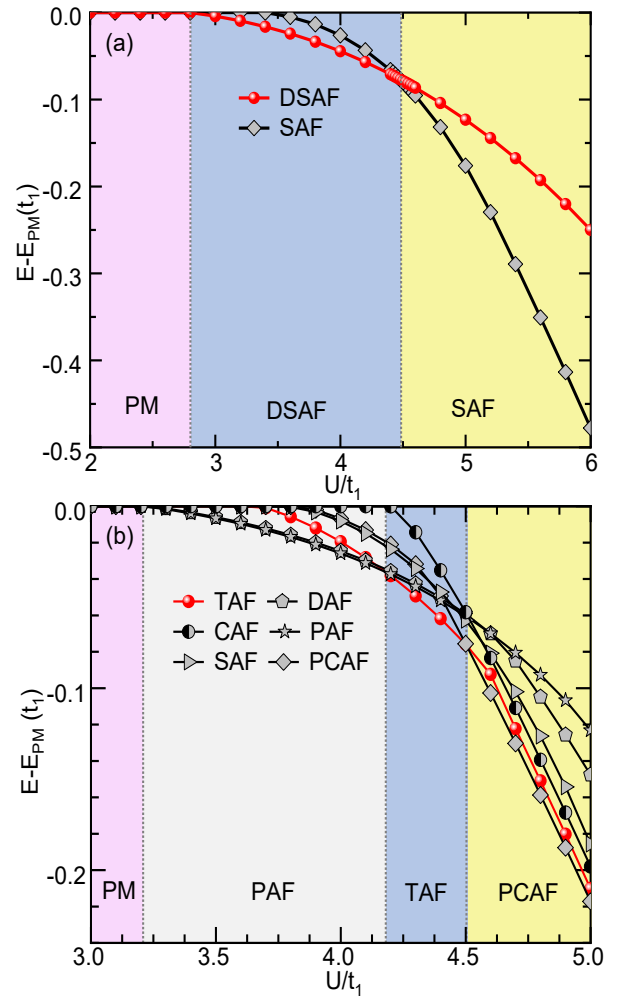


FIG. 5. (a) The free energies of SAF and DSAF as functions of the on-site Coulomb interaction U at $t_2/t_1 = 0.99$, where the energy of the paramagnetic state is set to zero. (b) The free energies of CAF, DAF, TAF, PCAF, PAF and SAF as functions of U at $t_2/t_1 = 0.765$, where the energy of the paramagnetic state is set to zero.

condition is used. Since particles, namely the magnetic configurations, will ultimately converge to the position where the free energy is minimized regardless of their initial positions within the framework of this algorithm, we initialize the magnetic configurations randomly and update them iteratively following the flowchart as shown in Fig.1. Notably, two new magnetic states, namely DSAF and TAF, are found apart from the existing states of CAF, DAF, PAF, PCAF, and SAF, where DSAF is in the region of weak geometrical frustration while TAF locates at strong geometrical frustration region. Interestingly, a Hubbard model with only the nearest and next-nearest neighbour hoppings can favor TAF, whereas J_1, J_2, J_3 , and K are needed for a Heisenberg model²². The specific configurations of DSAF and TAF are shown in Fig.4(a) and 4(b), respectively. It is necessary to mention that the calculations here are performed on a finite size with

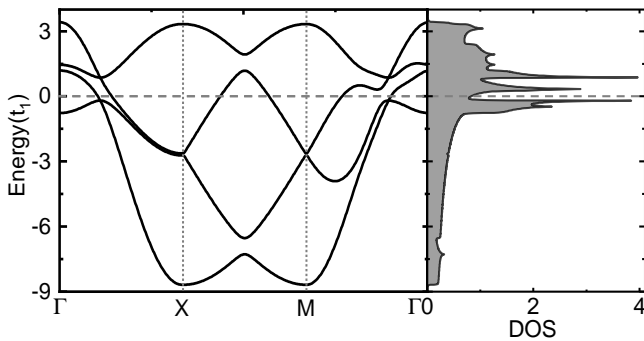


FIG. 6. Band structure and corresponding DOS for the DSAF state at $t_2/t_1 = 0.99$ and $U/t_1 = 3.6$.

only 24×24 , which may be affected by finite-size effects.

To confirm that these two new magnetic states are not a result of a finite-size effect, we further perform mean-field calculations in the thermodynamical limit. Figure 5 shows the comparison of free energies between DSAF and its corresponding competing states 5(a), as well as between TAF and its corresponding competing states 5(b). Obviously, DSAF occurs in the region between the paramagnetic state (PM) and SAF, while TAF exists in the region between PAF and PCAF. Thus, the presence of our two new found magnetic states is confirmed in the thermodynamical limit, which is not a result of a finite-size effect.

Considering that DSAF occurs at $2.8 < U/t_1 < 4.5$ ($0.23 < U/W < 0.36$, where W is the bandwidth) for $t_2/t_1 = 0.99$, where geometrical frustration is released and the electronic correlation is relatively weak, this state may be reliable within mean-field approximation. Thus, we investigate the band structure and density of states (DOS) for DSAF in Fig. 6. As can be seen, DSAF is metallic. Furthermore, we demonstrate the magnetic moments of DSAF and its corresponding competing states as a function of the on-site Coulomb interaction U at $t_2/t_1 = 0.99$ in Fig. 7 (a). The sudden enhancements of the magnetic moments from PM to DSAF and from DSAF to SAF suggest first-order phase transitions. The kink occurring in the magnetic moment for the case of SAF is a result of phase transition from metallic SAF to insulating SAF, consistent with previous study¹⁸. We also present a schematic phase diagram of DSAF in Fig. 7 (b). Obviously, DSAF becomes the ground state within a broad region for the magnetic states we considered.

IV. DISCUSSION

Here, we have proposed a new idea about how to search for magnetic ground states of the Hubbard model using PSO based on mean-field approximation by viewing magnetic configurations as particles. We have found two new magnetic ground states in the Hubbard model with the nearest and next-nearest neighbour hoppings by em-

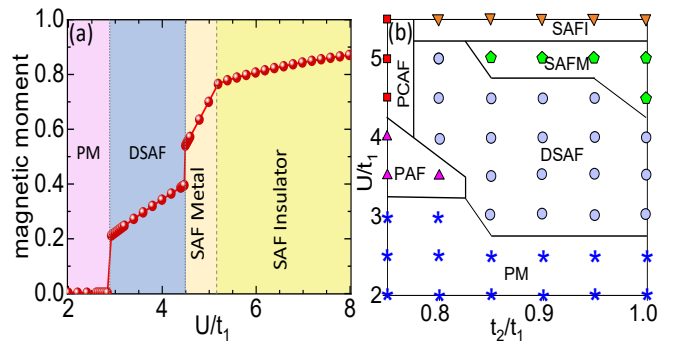


FIG. 7. (a) The magnetic moment as a function of the on-site Coulomb interaction U at $t_2/t_1 = 0.99$. (b) A schematic phase diagram of DSAF in the region of $0.75 < t_2/t_1 < 1$ and $2 < U/t_1 < 5.5$, in which the star, square, triangle, inverted triangle, pentagon, and circle denote PM, PCAF, PAF, SAFI, SAFM, and DSAF, respectively.

ploying our improved version of PSO. Although the PSO calculations in this paper are based on mean-field approximation, PSO is a very powerful algorithm that can be effectively combined with higher-level approximations to handle the Hubbard model, such as Hubbard-I approximation⁴², Hubbard-III approximation⁴³, projective operator approximation^{44,45}, coherent potential approximation⁴⁶⁻⁴⁸, dynamical mean-field theory^{49,50}, etc.

Twisting often leads to the emergence of exotic magnetic phases in layered materials, such as the coexistence of interlayer ferromagnetic and interlayer antiferromagnetic states in twisted bilayer CrI_3 ⁵¹. However, enumerating all the possible magnetic states in twisted layered materials becomes challenging due to the large number of sublattices in the supercell. Fortunately, PSO offers an excellent platform to automatically search for the magnetic ground state without the need for manual preparation of magnetic configurations. Therefore, the application of PSO in studying the magnetism of twisted systems is expected to be very interesting.

By using PSO, we have discovered two new magnetic states in the Hubbard model we investigated, including DSAF and TAF. Although a double-Q coplanar spin-vortex crystal phase is proposed when $t_2 \approx t_1$ and $U/W > 0.31$ ($U/t_1 > 3.8$)⁵², our DSAF occurs at the region with a weaker correlation interaction of $U/W > 0.23$ ($U/t_1 > 2.8$). Besides, since the geometrical frustration is released and the electronic correlation is weak, mean field approximation is reliable, as evidenced by qualitative consistencies between solutions from mean field approximation²¹ and VCA¹⁶ where SAF starts to appear at U/t_1 less than 4 if DSAF is not taken into account, indicating that quantum fluctuations completely ignored in mean field approximation are suppressed in the large t_2/t_1 and weak U/W region. Since the free energy of DSAF is significantly lower than that of other states in the DSAF phase, it is expectable that the stable DSAF solution should survive against the quantum fluctuations as even the metastable SAF solution has already sur-

vived against the quantum fluctuations¹⁶. Additionally, we find that a prominent peak is present in the vicinity of $(\pi/2, 0)$ for the Pauli susceptibility in the $t_2 \approx t_1$ region, indicating a tendency towards DSAF if perturbation, like the on-site Coulomb interaction, is switched on, further supporting our finding of DSAF in the certain region. Thus, DSAF is most probably a genuine ground state in a sufficient large parameter space for this Hubbard model even if both non-collinear magnetism and quantum fluctuations are considered. In contrast, TAF may be controversial since it occurs in the region of strong geometric frustration where macroscopic degeneracies dramatically affect the magnetism of the one-band Hubbard model. As a result, various competing states are proposed in this region, such as PCAF^{19,20}, DAF²¹, PAF²¹, as well as nonmagnetic insulating state¹⁹. Thus, it is interesting to use a more sophisticated method than mean-field approximation to confirm the stability of TAF over its corresponding competing states.

Compared to standard PSO, our improved PSO exhibits a higher performance because the search direction of particles in the standard PSO is so random that it lacks sufficient guidance. In contrast, by proposing an improved version of the learning factors and inertia weight, particles have their own characters to recognize the searching direction in our improved PSO, which significantly save the time of particles wandering around local optimum. Thus, our improved PSO converges faster than standard PSO. Our work provides valuable insights

into how to improve PSO by modifying the learning factors and inertia weight and demonstrates its effectiveness in searching new states of matters.

V. CONCLUSION

In conclusion, we have proposed an improved version of PSO, which converges to global optimum faster than standard PSO. By employing this improved PSO to search for new magnetic states in the Hubbard model with the nearest and next-nearest neighbour hoppings on the real-space square lattice with a finite size of 24×24 based on the mean-field approximation, two new magnetic states, including DSAF and TAF, are found. The presence of these two states in this Hubbard model is further confirmed by mean-field calculations in the thermodynamical limit, where the band structure, DOS, and magnetic moment of DSAF are also present.

VI. ACKNOWLEDGEMENT

This work is supported by National Natural Science Foundation of China (Grants No. 12274324, No. 12004283) and Shanghai Science and Technology Commission (Grant No. 21JC405700).

* These authors contribute equally to the paper.

† Corresponding author: yzzhang@tongji.edu.cn

- ¹ S. Li, C. de La Cruz, Q. Huang, Y. Chen, J.W. Lynn, J. Hu, Y.L. Huang, F.C. Hsu, K.W. Yeh, M.K. Wu, and P. Dai, "First-order magnetic and structural phase transitions in $\text{Fe}_{1+y}\text{Se}_x\text{Te}_{1-x}$," *Physical Review B* **79**, 054503 (2009).
- ² D.W. Tam, H.H. Lai, J. Hu, X. Lu, H.C. Walker, D.L. Abernathy, J.L. Niedziela, T. Weber, M. Enderle, Y. Su, Z.Q. Mao, Q. Si, and P. Dai, "Plaquette instability competing with bicollinear ground state in detwinned FeTe," *Physical Review B* **100**, 054405 (2019).
- ³ Y. Zhou, L. Miao, P. Wang, F.F. Zhu, W.X. Jiang, S.W. Jiang, Y. Zhang, B. Lei, X.H. Chen, H.F. Ding, *et al.*, "Antiferromagnetic order in epitaxial FeSe films on SrTiO_3 ," *Physical review letters* **120**, 097001 (2018).
- ⁴ Hai-Yuan Cao, Shiyong Chen, Hongjun Xiang, and Xin-Gao Gong, "Antiferromagnetic ground state with pair-checkerboard order in FeSe," *Physical Review B* **91**, 020504(R) (2015).
- ⁵ A.E. Taylor, S.J. Sedlmaier, S.J. Sedlmaier, S.J. Cassidy, E.A. Goremychkin, R.A. Ewings, T.G. Perring, S.J. Clarke, and A.T. Boothroyd, "Spin fluctuations away from $(\pi, 0)$ in the superconducting phase of molecular-intercalated FeSe," *Physical Review B* **87**, 220508 (2013).
- ⁶ A.E. Taylor, R.A. Ewings, T.G. Perring, J.S. White, P. Babkevich, A. Krzton-Maziopa, E. Pomjakushina, K. Conder, and A.T. Boothroyd, "Spin-wave excitations

- and superconducting resonant mode in $\text{Cs}_x\text{Fe}_{2-y}\text{Se}_2$," *Physical Review B* **86**, 094528 (2012).
- ⁷ Clarina de La Cruz, Q. Huang, J.W. Lynn, Jiyong Li, W. Ratcliff II, Jerel L Zarestky, HA Mook, GF Chen, JL Luo, NLa Wang, *et al.*, "Magnetic order close to superconductivity in the iron-based layered $\text{LaO}_{1-x}\text{F}_x\text{FeAs}$ systems," *nature* **453**, 899–902 (2008).
- ⁸ Q. Huang, Y. Qiu, W. Bao, M.A. Green, J.W. Lynn, Y.C. Gasparovic, T. Wu, G. Wu, and X.H. Chen, "Neutron-Diffraction Measurements of Magnetic Order and a Structural Transition in the Parent BaFe_2As_2 Compound of FeAs-Based High-Temperature Superconductors," *Physical Review Letters* **101**, 257003 (2008).
- ⁹ S. Li, C. de La Cruz, Q. Huang, G.F. Chen, T.L. Xia, J.L. Luo, N.L. Wang, and P. Dai, "Structural and magnetic phase transitions in $\text{Na}_{1-\delta}\text{FeAs}$," *Physical Review B* **80**, 020504 (2009).
- ¹⁰ Premala Chandra, Piers Coleman, and AI Larkin, "Ising transition in frustrated Heisenberg models," *Physical review letters* **64**, 88 (1990).
- ¹¹ Fengjie Ma, Wei Ji, Jiangping Hu, Zhong-Yi Lu, and Tao Xiang, "First-principles calculations of the electronic structure of tetragonal α -FeTe and α -FeSe crystals: evidence for a bicollinear antiferromagnetic order," *Physical review letters* **102**, 177003 (2009).
- ¹² Samuel Ducatman, Natalia B Perkins, and Andrey Chubukov, "Magnetism in parent iron chalcogenides: Quantum fluctuations select plaquette order," *Physical re-*

- view letters **109**, 157206 (2012).
- 13 Jiangping Hu, Bao Xu, Wuming Liu, Ning-Ning Hao, and Yupeng Wang, “Unified minimum effective model of magnetic properties of iron-based superconductors,” *Physical Review B* **85**, 144403 (2012).
 - 14 Wei-Guo Yin, Chi-Cheng Lee, and Wei Ku, “Unified picture for magnetic correlations in iron-based superconductors,” *Physical review letters* **105**, 107004 (2010).
 - 15 S Yamaki, K Seki, and Y Ohta, “Ground-state phase diagram of the asymmetric Hubbard model with geometrical frustration,” *Physical Review B* **87**, 125112 (2013).
 - 16 A.H. Nevidomskyy, C. Scheiber, D. Sénéchal, and A.M.S. Tremblay, “Magnetism and d-wave superconductivity on the half-filled square lattice with frustration,” *Physical Review B* **77**, 064427 (2008).
 - 17 Luca F Tocchio, Federico Becca, Alberto Parola, and Sandro Sorella, “Role of backflow correlations for the nonmagnetic phase of the $t-t'$ Hubbard model,” *Physical Review B* **78**, 041101(R) (2008).
 - 18 Zeng-Qiang Yu and Lan Yin, “Collinear antiferromagnetic state in a two-dimensional Hubbard model at half filling,” *Physical Review B* **81**, 195122 (2010).
 - 19 Takahiro Mizusaki and Masatoshi Imada, “Gapless quantum spin liquid, stripe, and antiferromagnetic phases in frustrated Hubbard models in two dimensions,” *Physical Review B* **74**, 014421 (2006).
 - 20 A Yamada, K Seki, R Eder, and Y Ohta, “Magnetic properties and Mott transition in the square-lattice Hubbard model with frustration,” *Physical Review B* **88**, 075114 (2013).
 - 21 Ze Ruan, Xiu-Cai Jiang, Ze-Yi Song, and Yu-Zhong Zhang, “Uncovering double-stripe and plaquette antiferromagnetic states in the one-band hubbard model on a frustrated square lattice,” *New Journal of Physics* **23**, 053028 (2021).
 - 22 JK Glasbrenner, II Mazin, Harald O Jeschke, PJ Hirschfeld, RM Fernandes, and Roser Valentí, “Effect of magnetic frustration on nematicity and superconductivity in iron chalcogenides,” *Nature Physics* **11**, 953–958 (2015).
 - 23 Kazuma Misumi, Tatsuya Kaneko, and Yukinori Ohta, “Phase diagram of the frustrated square-lattice Hubbard model: variational cluster Approach,” *Journal of the Physical Society of Japan* **85**, 064711 (2016).
 - 24 James Kennedy and Russell Eberhart, “Particle swarm optimization,” in *Proceedings of ICNN’95-international conference on neural networks*, Vol. 4 (IEEE, 1995) pp. 1942–1948.
 - 25 Russell Eberhart and James Kennedy, “A new optimizer using particle swarm theory,” in *MHS’95. Proceedings of the sixth international symposium on micro machine and human science* (Ieee, 1995) pp. 39–43.
 - 26 Yanchao Wang, Jian Lv, Li Zhu, and Yanming Ma, “Crystal structure prediction via particle-swarm optimization,” *Physical Review B* **82**, 094116 (2010).
 - 27 Shunhong Zhang, Yawei Li, Tianshan Zhao, and Qian Wang, “Robust ferromagnetism in monolayer chromium nitride,” *Scientific reports* **4**, 5241 (2014).
 - 28 Xin Qu, Lihua Yang, Jian Lv, Yu Xie, Jinghai Yang, Yukai Zhang, Yanchao Wang, Jijun Zhao, Zhongfang Chen, and Yanming Ma, “Particle swarm predictions of a $StrB_3$ monolayer with 12-fold metal coordination,” *Journal of the American Chemical Society* **144**, 11120–11128 (2022).
 - 29 Shenshen Yan, Yan Liu, Zi Wang, Xiaohua Lan, Yi Wang, and Jie Ren, “Designing radiative cooling metamaterials for passive thermal management by particle swarm optimization,” *Chinese Physics B* **32**, 057802 (2023).
 - 30 Jayanti Prasad and Tarun Souradeep, “Cosmological parameter estimation using particle swarm optimization,” *Physical Review D* **85**, 123008 (2012).
 - 31 Andrés N Ruiz, Sofía A Cora, Nelson D Padilla, Mariano J Domínguez, Cristian A Vega-Martínez, Tomás E Tecce, Álvaro Orsi, Yamila Yaryura, Diego García Lambas, Ignacio D Gargiulo, *et al.*, “Calibration of semi-analytic models of galaxy formation using particle swarm optimization,” *The Astrophysical Journal* **801**, 139 (2015).
 - 32 Zahra Beheshti and Siti Mariyam Hj Shamsuddin, “CAPSO: centripetal accelerated particle swarm optimization,” *Information Sciences* **258**, 54–79 (2014).
 - 33 Maurice Clerc and James Kennedy, “The particle swarm-explosion, stability, and convergence in a multidimensional complex space,” *IEEE transactions on Evolutionary Computation* **6**, 58–73 (2002).
 - 34 Rui Mendes, James Kennedy, and José Neves, “The fully informed particle swarm: simpler, maybe better,” *IEEE transactions on evolutionary computation* **8**, 204–210 (2004).
 - 35 Amitava Chatterjee and Patrick Siarry, “Nonlinear inertia weight variation for dynamic adaptation in particle swarm optimization,” *Computers & operations research* **33**, 859–871 (2006).
 - 36 Yu Wang, Bin Li, Thomas Weise, Jianyu Wang, Bo Yuan, and Qiongjie Tian, “Self-adaptive learning based particle swarm optimization,” *Information Sciences* **181**, 4515–4538 (2011).
 - 37 Andries Engelbrecht, “Particle swarm optimization: Velocity initialization,” in *2012 IEEE congress on evolutionary computation* (IEEE, 2012) pp. 1–8.
 - 38 Yuhua Li, Zhi-Hui Zhan, Shujin Lin, Jun Zhang, and Xiaonan Luo, “Competitive and cooperative particle swarm optimization with information sharing mechanism for global optimization problems,” *Information Sciences* **293**, 370–382 (2015).
 - 39 M Munlin and M Anantathanavit, “New social-based radius particle swarm optimization,” in *2017 12th IEEE Conference on Industrial Electronics and Applications (ICIEA)* (IEEE, 2017) pp. 838–843.
 - 40 Jiehong Wu, Chengxin Song, Chunlong Fan, Ammar Hawbani, Liang Zhao, and Xichun Sun, “Denpso: A distance evolution nonlinear pso algorithm for energy-efficient path planning in 3d uasns,” *IEEE access* **7**, 105514–105530 (2019).
 - 41 Johannes Jakubik, Adrian Binding, and Stefan Feuerriegel, “Directed particle swarm optimization with Gaussian-process-based function forecasting,” *European Journal of Operational Research* **295**, 157–169 (2021).
 - 42 John Hubbard, “Electron correlations in narrow energy bands,” *Proceedings of the Royal Society of London. Series A. Mathematical and Physical Sciences* **276**, 238–257 (1963).
 - 43 John Hubbard, “Electron correlations in narrow energy bands III. An improved solution,” *Proceedings of the Royal Society of London. Series A. Mathematical and Physical Sciences* **281**, 401–419 (1964).
 - 44 Laura M Roth, “Electron correlation in narrow energy bands. I. The two-pole approximation in a narrow S band,” *Physical Review* **184**, 451 (1969).

- ⁴⁵ Peng Fan, Ke Yang, Kou-Han Ma, and Ning-Hua Tong, “Projective truncation approximation for equations of motion of two-time Green’s functions,” *Physical Review B* **97**, 165140 (2018).
- ⁴⁶ Paul Soven, “Coherent-potential model of substitutional disordered alloys,” *Physical Review* **156**, 809 (1967).
- ⁴⁷ B Velický, S Kirkpatrick, and H Ehrenreich, “Single-site approximations in the electronic theory of simple binary alloys,” *Physical Review* **175**, 747 (1968).
- ⁴⁸ Jin-Rong Xu, Ze-Yi Song, Hai-Qing Lin, and Yu-Zhong Zhang, “Gate-induced gap in bilayer graphene suppressed by Coulomb repulsion,” *Physical Review B* **93**, 035109 (2016).
- ⁴⁹ Antoine Georges and Gabriel Kotliar, “Hubbard model in infinite dimensions,” *Physical Review B* **45**, 6479 (1992).
- ⁵⁰ Antoine Georges, Gabriel Kotliar, Werner Krauth, and Marcelo J Rozenberg, “Dynamical mean-field theory of strongly correlated fermion systems and the limit of infinite dimensions,” *Reviews of Modern Physics* **68**, 13 (1996).
- ⁵¹ Yang Xu, Ariana Ray, Yu-Tsun Shao, Shengwei Jiang, Kihong Lee, Daniel Weber, Joshua E Goldberger, Kenji Watanabe, Takashi Taniguchi, David A Muller, *et al.*, “Co-existing ferromagnetic–antiferromagnetic state in twisted bilayer CrI_3 ,” *Nature Nanotechnology* **17**, 143–147 (2022).
- ⁵² Yun-Peng Huang, Jin-Wei Dong, Panagiotis Kotetes, and Sen Zhou, “Antiferromagnetic chiral spin density wave and strain-induced Chern insulator in the square lattice Hubbard model with frustration,” *Physical Review B* **102**, 195120 (2020).